Journal of Alloys and Compounds 520 (2012) 158–163

Contents lists available at SciVerse ScienceDirect

Journal of Alloys and Compounds

journal homepage: www.elsevier.com/locate/jallcom

Effect of oxygen pressure on the structural, optical and magnetic properties of pulsed laser ablated ZnCoO thin films

C.C. Wang, M. Liu, B.Y. Man*, C.S. Chen, S.Z. Jiang, S.Y. Yang, X.G. Gao, S.C. Xu, B. Hu, Z.C. Sun

College of Physics and Electronics, Shandong Normal University, Jinan 250014, PR China

ARTICLE INFO

Article history:
Received 13 November 2011
Accepted 30 December 2011
Available online 9 January 2012

Keywords:
ZnCoO thin film
CoO phase
Point defect

ABSTRACT

Wurtzite structure ZnCoO thin films with *c*-axis preferential orientation were synthesized on *c*-plane sapphire substrates by using pulsed laser deposition (PLD) technique under various oxygen pressures. The structural, optical and magnetic properties of the films were investigated. When the oxygen pressure was relatively low (<1.3 Pa), the cobalt was incorporated in the ZnO lattice as Co^{2+} and substituted for Zn site with no evidence of any impurity phase, whereas inhomogeneous films of wurtzite ZnO phase mixed with cubic CoO phase formed when oxygen pressure was high. The experimental results show that the magnetic behavior is directly related to the presence of intrinsic defects. By changing oxygen pressure to control the amount of Zn vacancies, zinc interstitials and oxygen vacancies, ferromagnetism can be tuned significantly, which is a direct evidence that these defects play an important role in mediating the ferromagnetism in Co-doped ZnO thin films.

1. Introduction

There is currently a lot of interest in the science and potential technological applications of spintronics, which combine both charge and spin degrees of freedom in a single substance. In particular, so called dilute magnetic semiconductors (DMSs) have been investigated as their promising application in spintronics devices [1]. Zinc oxide (ZnO) is a direct band gap II–IV compound semiconductor with wurtzite type structure. Its high band gap energy (3.37 eV) and large excitonic binding energy (60 meV) at room temperature, make it a potential candidate for ultraviolet optoelectronic devices such as light emitting diodes, laser and photodetectors [2]. ZnO has received much attention due to the ease with which carriers and magnetic dopants may be introduced into the material, and many studies focus on Co-doped ZnO [3]. Many reports on the observation of ferromagnetism at room temperature have been published, while surprisingly other reports did not evidence any ferromagnetism in the compounds [4–6]. There is a continuous debate about the origin of ferromagnetism and it is not clear whether ferromagnetism is originated from clusters, secondary phases, or it is an intrinsic phenomenon. Some researchers suggested that the observed magnetic property is due to the presence of cobalt microclusters in cobalt-doped ZnO thin films [7]. However, others have proposed that the ferromagnetism is due to the Ruderman–Kittel–Kasuya–Yosida indirect exchange or double exchange mechanism [8,9], or the percolation of bound magnetic polarons (BMPs) [10].In order to further research structural, optical and magnetic properties of Co-doped ZnO, we fabricated ZnCoO thin films on sapphire substrates by pulsed laser deposition (PLD) technique under different oxygen pressure from 10^{-4} to 5 Pa. In this article, we are concerned with the relationship between growth conditions and properties of ZnCoO thin films.

2. Experiment procedure

$Zn_{0.95}Co_{0.05}O$ thin films were grown on *c*-plane sapphire substrates under different oxygen pressures by PLD. The $Zn_{0.95}Co_{0.05}O$ target was prepared by the conventional solid state reaction technique. ZnO (99.99%) powder and Co_2O_3 (99.9%) powder as raw materials were mixed for 6 hours using a ball-mill, then uniaxially pressed (200 MPa) into a disk. The corresponding target was continuously sintered at 800 °C, 1000 °C and 1200 °C for 2 h in air and then quenched to room temperature finally [11]. The chamber was evacuated by a turbomolecular pump to a base pressure of 10^{-5} Pa. A pulsed KrF excimer laser with a wavelength of 248 nm, a frequency of 10 Hz and energy of 200 mJ was used for deposition. The deposition period was 15 min. The pressure of the ambient oxygen gas for thin film growth was varied from 10^{-4} to 5 Pa with the substrate temperature kept at 500 °C. The thicknesses of the films grown were 200–300 nm.

The crystal structure of the thin films was characterized by conventional x-ray diffraction (XRD, D/Max-2400) using Cu Kα radiation. The composition was investigated by Energy dispersive spectroscopy (EDS, Oxford X-Max). The oxidation state of the Co ions was studied by X-ray photoelectron spectroscopy (XPS, PHI-5300). The surface morphology was characterized by atomic force microscope (AFM, PARK Autoprobecp). The optical transmittance spectra were obtained by a UV-vis-NIR spectrophotometer (U-4000) in the wavelength range from 300 to 800 nm. Raman spectroscopy (LabRAM-HR800) as a nondestructive characterization was used to study the substitution in the host lattice and identify the impurity phases. The photoluminescence (PL, FLS-920) were measured with an excitation wavelength of 300 nm. The magnetic properties of the thin films were measured by an

* Corresponding author. Tel.: +86 531 8618 0027; fax: +86 531 8618 0804.
E-mail address: byman@sdnu.edu.cn (B.Y. Man).

0925-8388/$ – see front matter.
doi:10.1016/j.jallcom.2011.12.170

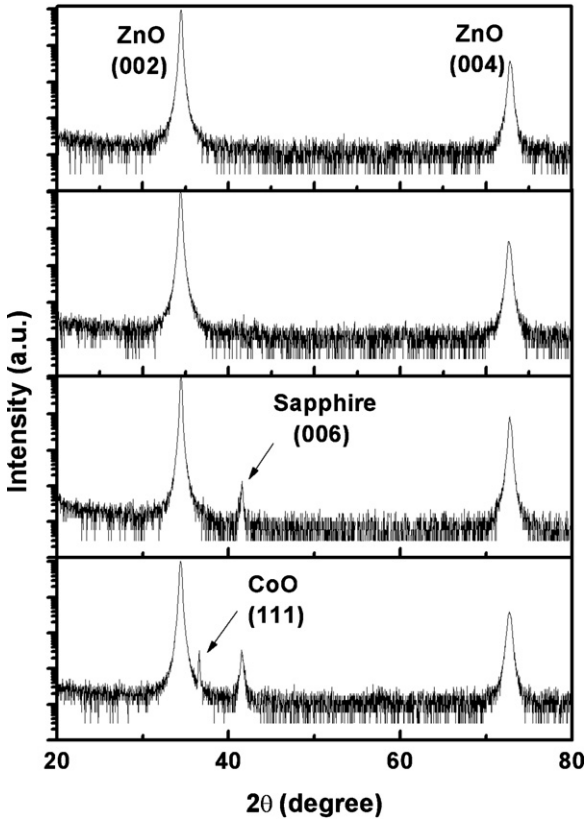

Fig. 1. XRD scans for a series of ZnCoO films grown under different oxygen pressures on *c*-plane sapphire substrates shown on a log scale. The films are predominantly *c*-axis orientation.

alternating gradient magnetometer (AGM, MicroMag Mode 2900) with a resolution of 1×10^{-8} emu. All measurements were carried out at room temperature.

3. Results and discussion

Fig. 1 shows XRD patterns of ZnCoO thin films grown on sapphire substrates under different growth conditions. The strong intensities of the (0 0 2) and (0 0 4) peaks indicate that the thin films grown over a wide range of oxygen pressures are highly *c* axis oriented. We found that homogeneous ZnCoO thin films with a single phase wurtzite structure grow when the oxygen pressure is relatively low at 500 °C. In contrast, when the oxygen pressure is relatively high (≥1.3 Pa), we observed diffractions from cubic CoO phase in the XRD patterns, as shown in Fig. 1. We note that the crystal orientations of the CoO particles are dominantly (1 1 1), suggesting specific preferential alignment of particles in ZnO matrix, which is also in good accordance with other experimental results [12]. The Co content dependence of the *c*-axis lattice constants is shown in Fig. 2. The *d* (0 0 2) value of the ZnCoO thin films increases almost lonely as a function of the Co doping content, implying that Co is systematically substituted for Zn in the films. And this result is consistent with the observation by Ueda et al. [8]. The large deviation from the *d* value of the film grown 1.3 Pa oxygen pressure is ascribed to reduction of the Co concentration in the wurtzite phase due to the segregation of CoO.

EDS is used to measure the percentage of cobalt in the ZnCoO films. Inset (a) in Fig. 2 shows the cobalt concentration in the films deposited under different oxygen pressures. In all cases, the dopant concentration in the film is higher than in the target. Similar results of the transition metal enrichment in doped ZnO films grown by PLD have been reported [13–15]. The reasons have been analyzed by the higher sputter yield of the Zn atoms than Co atoms from the

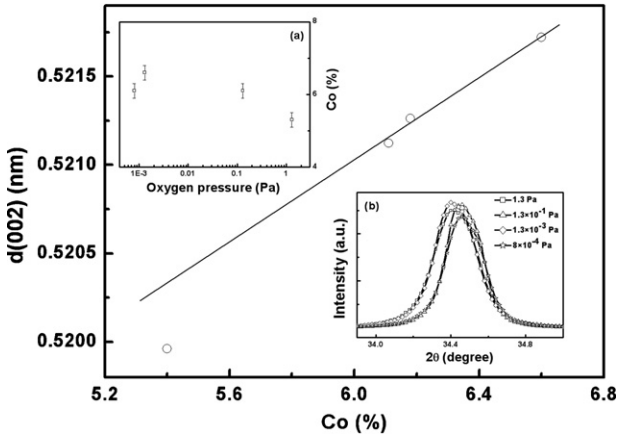

Fig. 2. Evolution of the lattice parameter in ZnCoO thin films as a function of the Co content. Inset (a) EDS results for ZnCoO thin films grown under different oxygen pressures at 500 °C. Inset (b) the rocking curves (ω scan) of (0 0 2) reflection of the films.

thin film surface, which caused by the high energy ions (several hundred eV) in the laser ablation plasma plume [14].

XPS studies are made to obtain the information of the possible oxidation states of cobalt in the ZnO films. Fig. 3 shows the Zn and Co core level XPS spectra of the ZnCoO sample grown under 1.3×10^{-3} Pa after removal of 5 nm of the surface material by Ar^+ sputtering. It reveals that the Zn 2p peak is very sharper and the corresponding bonding-energy of Zn $2p_{3/2}$ and $2p_{1/2}$ are around 1021.1 and 1044.2 eV, respectively, pointing to Zn^{2+}. The Co 2p spectrum shows four peaks, the $2p_{3/2}$ and $2p_{1/2}$ doublet and shake-up resonance transitions (satellite) of these two peaks at higher binding energies. The satellite structure result from the charge-transfer band structure characteristic of the late 3d transition metal monoxides [16]. The Co $2p_{3/2}$ core levels for Co—O bonding at 781.0 eV, and the energy difference between Co$2p_{3/2}$ and Co $2p_{1/2}$ is 15.4 eV, which matches that of standard CoO, indicating the presence of a high-spin divalent state of Co in these samples [17]. Thus, within the detection limits of the spectrometer, we can rule out metallic Co as the source of the observed ferromagnetism.

Fig. 4 displays three-dimensional surface morphology images of ZnCoO thin films deposited under different oxygen pressures. The scanning area was 1 μm × 1 μm. The surfaces of the films are dense and smooth, also show preferred *c*-axis orientation. The root mean square (RMS) of samples deposited under 1.3 Pa, 1.3×10^{-1} Pa, 1.3×10^{-3} Pa and 8×10^{-4} Pa, determined by the

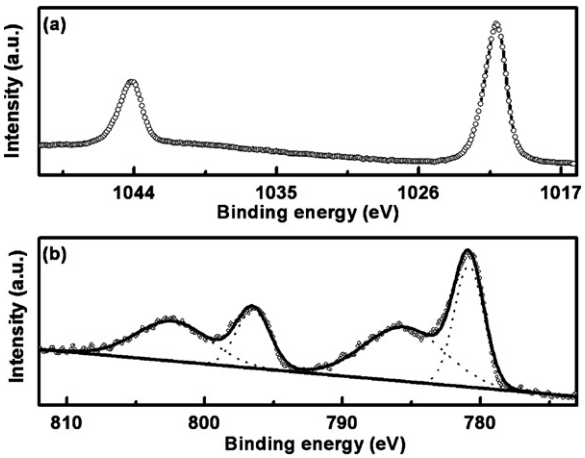

Fig. 3. Zn and Co 2p XPS spectrum of the ZnCoO samples after sputtering with 4 keV Ar+ ions at an angle of 45° relative to the film surface.

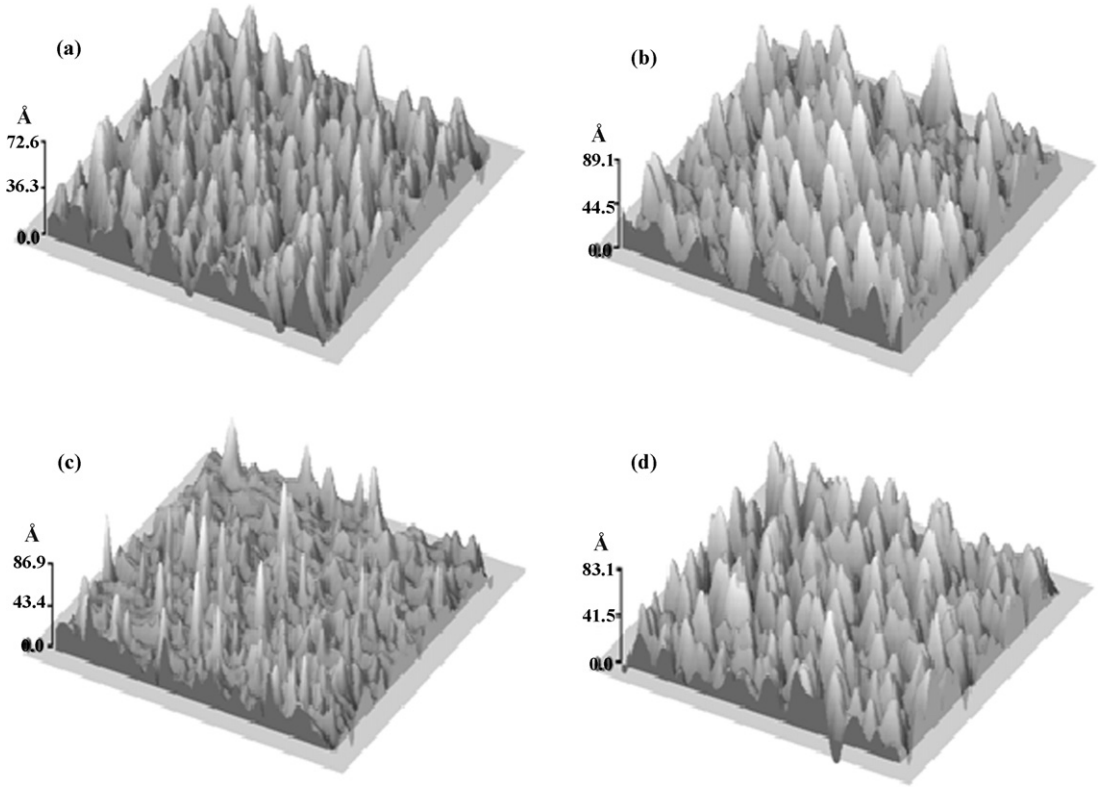

Fig. 4. Three-dimensional surface morphology images of ZnCoO thin films deposited under various oxygen pressures (a) 1.3 Pa, (b) 1.3×10^{-1} Pa, (c) 1.3×10^{-3} Pa and (d) 8×10^{-4} Pa.

AFM measurements, was 1.46 nm, 1.64 nm, 1.18 nm and 1.78 nm, respectively. Moreover, we could see that island-like grains which are due to the 3D columnar growth [18] completely covered the whole film surface.

The thickness-corrected optical transmittance spectra as a function of wavelength of the ZnCoO samples are shown in Fig. 5. The transmittance spectra for all ZnCoO thin films show an average transmittance about 80% in the region from 450 to 800 nm indicating excellent crystalline quality and optical properties. In addition

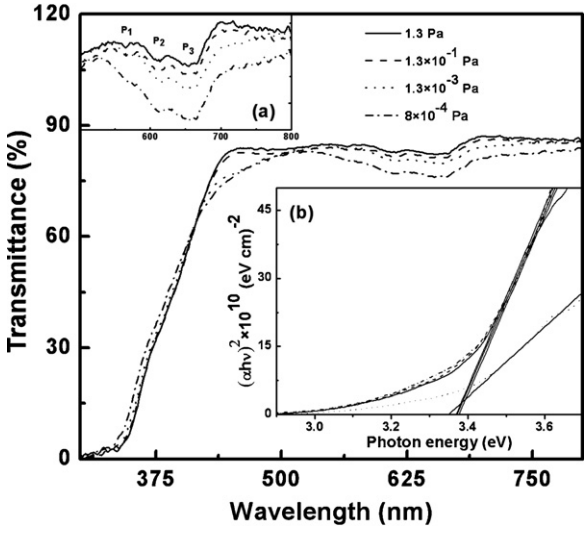

Fig. 5. Room temperature optical transmittance spectrum for ZnCoO thin films grown under different oxygen pressures. The inset (a) shows a close-up view of the absorption peaks corresponding to Co^{2+} in wurtzite ZnO. The inset (b) shows optical bandgap plots for ZnCoO films.

to the band gap absorption, three absorption peaks are observed at approximately 566, 611 and 655 nm labeled as P_1, P_2 and P_3, respectively (as shown in inset (a)), which can be identified as the d-d transitions of Zn substituted Co^{2+} ions from the $^4A_2(E)$ ground state toward $^2A_1(G)$, $^4T_1(P)$ and $^2E(G)$ excited states [19,20]. This shows that the Co ion has the valence state of +2 in the tetrahedral crystal field of the ZnO lattice, which is consistent with the result of XPS. In the spectra of the samples deposited under higher (1.3 and 1.3×10^{-1} Pa) and lower (1.3×10^{-3} and 8×10^{-4} Pa) oxygen pressure significant different variations are observed over the wavelength range of 430–510 nm. This difference may be attributed to the difference in the number of point defects, such as oxygen vacancies and/or interstitial Zn atoms. The optical bandgap values determined using Tauc relationship [21] as follows:

$$\alpha h\nu = A(h\nu - E_g)^{1/2}$$

where α is the absorption coefficient, $h\nu$ is the photon energy, A is a parameter with the transition probability and E_g is the optical bandgap. The bandgap was calculated by plotting $(\alpha h\nu)^2$ versus $h\nu$ and extrapolating the linear portion of the plot to $(\alpha h\nu)^2 = 0$ as shown in the inset (b). For the ZnCoO films deposited under 1.3, 1.3×10^{-1} and 8×10^{-4} Pa, the estimated optical bandgap are about 3.37 eV. For the sample deposited under 1.3×10^{-3} Pa, the estimated optical bandgap are about 3.35 eV. The obvious red-shift for the sample deposited under 1.3×10^{-3} Pa could be attributed to the sp-d exchange between the ZnO band electrons and localized d-electrons associated with the doped Co cations. This interaction leads to corrections in the energy bands; the conduction band is lowed and the valence band is raised causing the bandgap to shrink [22].

The Raman measurements are performed in the backscattering geometry at room temperature with a 473 nm laser as an excitation source. A liquid-N_2-cooled charge-coupled device detector

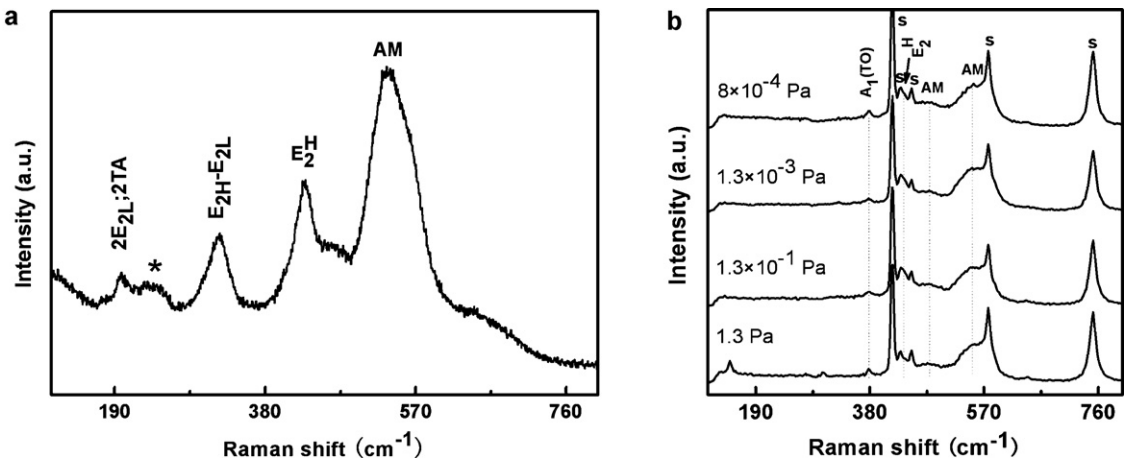

Fig. 6. (a) Room temperature Raman spectra of $Zn_{0.95}Co_{0.05}O$ target. (b) Room temperature Raman spectra of ZnCoO thin films deposited under different oxygen pressures on sapphire substrates (s).

is used to collect the scattered photons. The Raman spectra of the $Zn_{0.95}Co_{0.05}O$ target are dominated by five broad peaks, as shown in Fig. 6(a). The peaks at 198, 322 and 429 cm^{-1} can be attributed to the $2E_{2L}$; 2TA, E_{2H}-E_{2L} and E_{2H} modes, respectively. The vibrations at around 230 cm^{-1} (labeled with *) is assigned to the acoustic-phonon branch at the zone boundary and the additional mode centered at 540 cm^{-1} is observed due to Co substitution [23]. Fig. 6(b) shows the spectra of Co-doped ZnO deposited under different oxygen pressure. The peaks at 378 and 437 cm^{-1} can be attributed to the A_1(TO) and E_2^{high} modes, respectively [24]. In addition to the strong phonon modes from the sapphire substrate (the peaks labeled with 's'), additional broad modes are observed at around 480 cm^{-1} and 549 cm^{-1}, which are attributed to the Co substitution [23]. A similar multiphonon band in the range of 500–600 cm^{-1} was also reported for P^+ implanted ZnO, which was attributed to the defect induced band. They have also shown that after annealing the intensity of this multiphonon mode was reduced [25]. It also should be noted that for the sample deposited under 1.3 Pa oxygen pressure, additional weak peaks at about 146 cm^{-1} and 300 cm^{-1} appear in the spectrum, which are

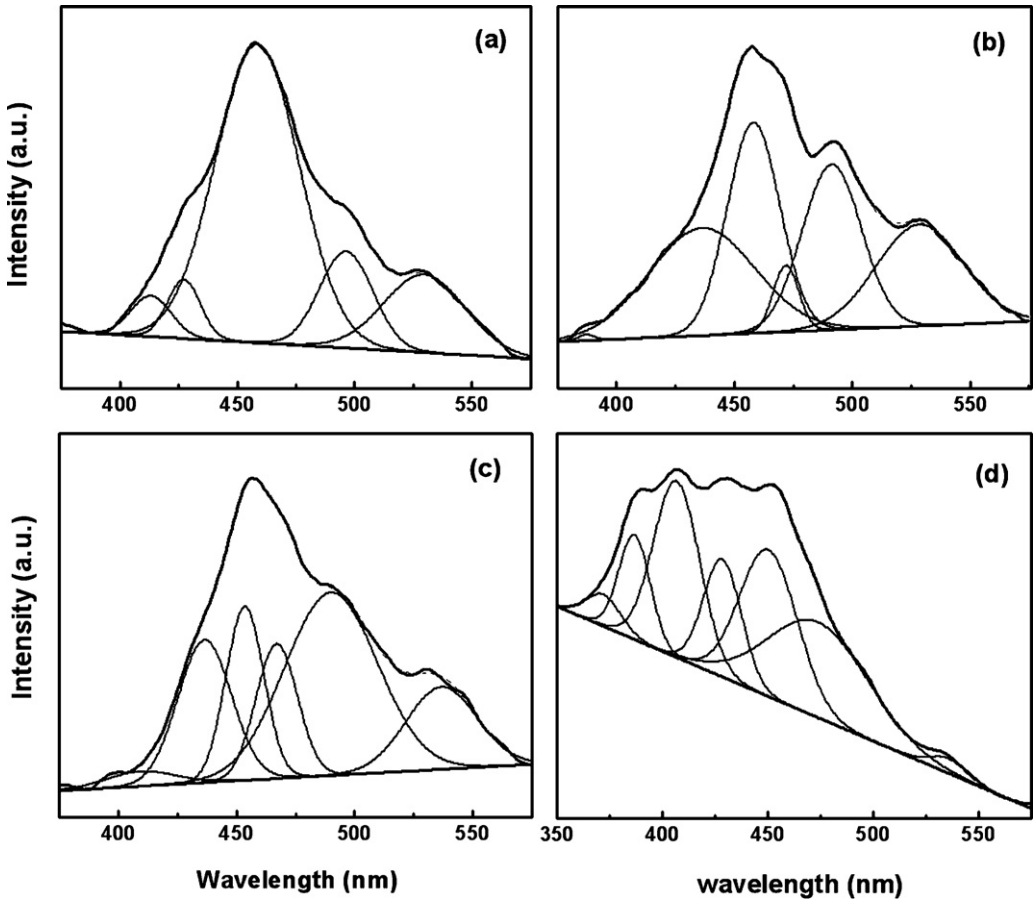

Fig. 7. Room temperature PL spectra of ZnCoO thin films grown under different oxygen pressures (a) 8×10^{-4} Pa, (b) 1.3×10^{-3} Pa, (c) 1.3×10^{-1} Pa, (d) 1.3 Pa.

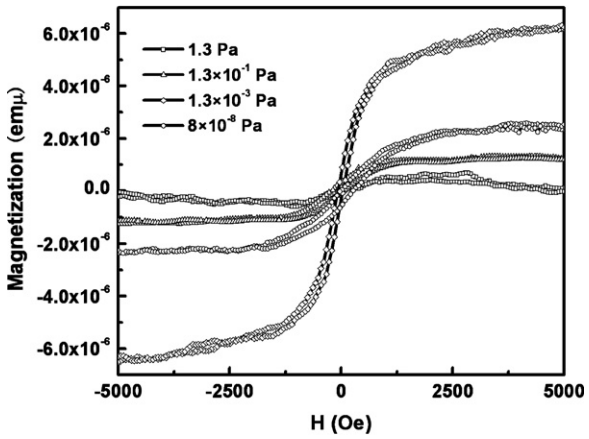

Fig. 8. Room temperature AGM magnetization curves for films deposited under different oxygen pressures. The measurements of magnetic properties were carried out with size 2 mm × 2 mm.

related to CoO mangnons [26,27]. The presence of such precipitate has also been found in bulk single crystals $Zn_{1-x}Co_xO$ ($x = 0.05$) [28]. And this is consistent with the XRD results.

PL can be used for investigating the defects in ZnO. We measured the PL spectra of ZnCoO thin films grown under different oxygen pressures, as shown in Fig. 7. For all the films, broad blue-green luminescence bands are visible across the spectra. The films are grown in low oxygen pressure and are non-stoichiometric which could give rise to the broad defect bands. The PL spectrum of the thin film grown under 1.3 Pa oxygen pressure varies greatly with the other samples, which may be duo to the presence of CoO clusters. The violet luminescence peak (~410 nm) was also observed in Mg-doped ZnO thin films by radio frequency reactive magnetron sputtering and explained by the electron transition from conduction band to shallow acceptor level formed by Zn vacancies [29]. According to calculated results of Kohan et al. [30], there existed a few transition mechanisms to generate the blue emission band in ZnO films: (1) the electron transition from shallow donor level formed by interstitial Zn atoms to the top of the valence band; (2) the electron transition from the conduction band to acceptor level formed by misplaced oxygen defects. It is well known that with the increment of oxygen pressure the zinc vacancies will increase, whereas interstitial Zn will decrease due to charge equilibrium. In our case, the intensity of blue emission band decreased with the oxygen pressure, indicating that the first mechanism is appropriate in our experiments. Blue emission peak occurred at about 490 nm and weak green emission peak occurred at about 530 nm were also observed. According to Xu's results [29], blue emission peak might originate from the electron transition from shallow donor level formed by interstitial Zn to shallow acceptor level formed by Zn vacancies. Kang et al. [31] concluded that the mechanism of green luminescence in ZnO was not by the transition from near band edge to deep acceptor level but by the transition from deep donor level by the oxygen vacancies to valence band. However, more investigations are needed to fully understand the origin of PL.

Fig. 8 shows the room-temperature AGM hysteresis loops for the Co-doped ZnO thin films deposited under different oxygen pressures, where the magnetic field is applied perpendicular to the surface plane and the diamagnetic background is linearly subtracted by the high field magnetization. The hysteresis loops of the samples clearly indicate that the as-grown ZnCoO thin films are ferromagnetism with Curie temperature Tc above room temperature. The coercive fields of samples deposited under 1.3×10^{-1}, 1.3×10^{-3} and 8×10^{-4} Pa are about 160, 70 and 130 Oe, respectively. But the sample grown under 1.3 Pa shows almost no ferromagnetism. This may be due to the presence of antiferromagnetic CoO clusters with the Néel temperature below room temperature in the sample.

Here, we briefly discuss possible origins of ferromagnetism in our samples. As discussed above, the Co is not metallic but in +2 state substituting for Zn. So the room-temperature ferromagnetism caused from secondary phases can be ruled out. According to the reports [32–34], we think that the ferromagnetism of the as-deposited samples originates from the ferromagnetic coupling between Co^{2+} through indirect exchange related to point defects, such as Zn vacancies, Zn interstitials and oxygen vacancies. The interaction between electrons of Co 3d and those point defects changes the state density of Co 3d, i.e. the interaction changes the breadth of down-spin orbit of 3d. Consequently, the magnitude of ferromagnetism varied with these point defects. Different oxygen pressure lead to different densities of these point defects during the growth of the thin films, so the magnetic properties of the films varied with oxygen pressure. However, the relation between the magnetic property and density of defects is worth further research.

4. Conclusions

In conclusion, Co-doped ZnO thin films were prepared on *c*-plane sapphire using plused laser deposition under different oxygen pressure. The films are highly *c*-axis oriented and exhibit room-temperature ferromagnetism. The structure together with optical and magnetic properties of the films was studied. The XRD pattern, Raman analysis, XPS and UV–vis demonstrated that when the samples grown under low oxygen pressure, the Co cations successfully entered into the hexagonal wurtzite structure and substituted for Zn cations sites in ZnO lattice. But when the oxygen pressure was relatively high (≥1.3 Pa), cubic CoO phase precipitated in the thin films. The experimental results demonstrate that the observed magnetic behavior is directly related to the presence of intrinsic defects, notably Zn vacancies, Zn interstitials and oxygen vacancies.

Acknowledgments

The authors are grateful for the financial support of the National Natural Science Foundation of China (11047161, 10874103) and the Postdoctoral Innovation Projects of Shandong (200903036).

References

[1] S.A. Wolf, D.D. Awschalom, R.A. Buhrman, J.M. Daughton, S. von Molnar, M.L. Roukes, A.Y. Chtchelkanova, D.M. Treger, Science 294 (2001) 1488.
[2] W. Iwamoto, P.G. Pagliuso, C. Rettori, Phys. Rev. B 73 (2006) 245213.
[3] Y.L. Liu, J.L. MacManus-Driscoll, Appl. Phys. Lett. 94 (2009) 022503.
[4] Z. Jin, T. Fukumura, M. Kawasaki, K. Ando, H. Saito, T. Sekiguchi, Y.Z. Yoo, M. Murakami, Y. Matsumoto, T. Hasegawa, H. Koinuma, Appl. Phys. Lett. 78 (2001) 3824.
[5] S. Kolesnik, B. Dsbrowski, J. Appl. Phys. 96 (2004) 5379.
[6] G. Lawes, S. Risbud, P. Ramirez, R. Seshadri, Phys. Rev. B 71 (2005) 045201.
[7] J.H. Park, M.G. Kim, H.M. Jang, S. Ryu, Y.M. Kim, Appl. Phys. Lett. 84 (2004) 1338.
[8] K. Ueda, H. Tabata, T. Kawai, Appl. Phys. Lett. 79 (2001) 988.
[9] D.A. Schwartz, D.R. Gamelin, Adv. Mater. 16 (2004) 2115.
[10] J.M.D. Coey, M. Venkatesan, C.B. Fitzgerald, Nat. Mater. 4 (2005) 173.
[11] S.Y. Yang, B.Y. Man, M. Liu, C.S. Chen, X.G. Gao, C.C. Wang, B. Hu, Physica B 405 (2010) 4027.
[12] J.H. Kim, H.J. Kim, D.J. Kim, Y.E. Ihm, W.K. Choo, J. Appl. Phys. 92 (2002) 6066.
[13] C.B. Fitzgerald, M. Venkatesan, J.G. Lunney, L.S. Dorneles, J.M.D. Coey, Appl. Surf. Sci. 247 (2005) 493.
[14] L.S. Dorneles, D. O'Mahony, C.B. Fitzgerald, F. McGee, M. Venkatesan, I. Stanca, J.G. Lunney, J.M.D. Coey, Appl. Surf. Sci. 248 (2005) 406.
[15] M. Ivill, S.J. Pearton, S. rawal, L. Leu, P. Sadik, R. Das, A.F. Hebard, M. Chisholm, J.D. Budai, D.P. Norton, New J. Phys. 10 (2008) 065002.
[16] G.A. Carson, M.H. Nassir, M.A. Langell, J. Vac. Sci. Technol. A 14 (1996) 1637.
[17] X.F. Wang, J.B. Xu, B. Zhang, H.G. Yu, J. Wang, X.X. Zhang, G.J. Yu, Q. Li, Adv. Mater. 18 (2006) 2476.
[18] I. Petrov, P.B. Barna, L. Hultman, J.E. Greene, J. Vac. Sci. Technol. A 21 (2003) S117–S128.

[19] P. Koidl, Phys. Rev. B 15 (1977) 2493.
[20] S. Ramachandran, A. Tiwari, J. Narayan, Appl. Phys. Lett. 84 (2004) 5255.
[21] M. Girtan, G. Folcher, Surf. Coat. Technol. 172 (2003) 242.
[22] Y.R. Lee, A.K. Ramdas, R.L. Aggarwal, Phys. Rev. B 10 (1988) 10600.
[23] X.F. Wang, J.B. Xu, X.J. Yu, K. Xue, J.G. Yu, X.J. Zhao, Appl. Phys. Lett. 91 (2007) 031908.
[24] C. Raman, A.-L. Esther, I. Jordi, A. Luis, Phys. Rev. B 75 (2007) 165202.
[25] K. Samanta, P. Bhattacharya, R.S. Katiyar, Phys. Rev. B 73 (2006) 245213.
[26] R.R. Hayes, C.H. Perry, Solid State Commun. 13 (1973) 1915–1917.
[27] H.-H. Chou, H.Y. Fan, Phys. Rev. B 13 (1973) 1915.
[28] M. Millot, J. Gonzalez, I. Molina, B. Salas, Z. Golacki, J.M. Broto, H. Rakoto, M. Goiran, J. Alloys Compd. 423 (2006) 224.
[29] P.S. Xu, Y.M. Sun, C.S. Shi, F.Q. Xu, H.B. Pan, Nucl. Instrum. Methods Phys. Res. B 199 (2003) 286.
[30] A.F. Kohan, G. Ceder, D. Morgan, Phys. Rev. B 61 (2000) 15019.
[31] H.S. Kang, J.S. Kang, J.W. Kim, S.Y. Lee, J. Appl. Phys. 95 (2004) 1246.
[32] K. Samanta, P. Bhattacharya, R.S. Katiyar, W. Iwamoto, P.G. Pagliuso, C. Rettori, Phys. Rev. B 73 (2006) 245213.
[33] P. Dutta, M.S. Seehra, S. Thota, J. Kumar, J. Phys.: Condens. Matter 20 (2008) 015218.
[34] J. Chen, G.J. Jin, Y.Q. Ma, Chin. Phy. Soc. 58 (2009) 2707.